Stabilization of laser beam alignment to an optical resonator by heterodyne detection of off-axis modes

Nicholas M. Sampas and Dana Z. Anderson

We demonstrate a method for real time alignment of a Gaussian beam to an optical resonator. While the frequency of a source laser is stabilized to a fundamental cavity mode resonance, phase modulation sidebands are applied at the off-axis mode frequencies. Asymmetrical transmission of the sideband at the frequency of each off-axis mode produces amplitude modulated optical signals and indicates the extent of the misalignments. Phase sensitive detection of these optical signals provides the error signals which are minimized by a control system that steers the input beam. In this way, optimum coupling of an injected source beam can be maintained to the fundamental mode of the resonator. This active alignment technique has demonstrated a sensitivity to tilts of 0.1 nrad/$\sqrt{\text{Hz}}$ and to lateral beam displacements of 0.08 nm/$\sqrt{\text{Hz}}$ in the ~1-Hz–1-kHz frequency range. These values correspond to 2 parts in $10^7/\sqrt{\text{Hz}}$ for both the far-field divergence angle and the beam waist size. Such performance is within a factor of 2 of the shot noise limitation of the error signal measurement for a detected power of 160 μW.

I. Introduction

A passive optical resonator often serves as a relative length standard to which a source laser frequency is stabilized. When the frequency stability requirements are stringent, the alignment between the source laser beam and the reference cavity becomes an issue. Wiggle of the beam, for example, will be translated into laser frequency variations by the frequency servo control electronics. This paper presents a discussion and a demonstration of a technique that actively maintains the alignment of a source laser beam to a passive resonator.

The effects of alignment fluctuations and drifts on a ring laser gyroscope were quantitatively observed by Sanders *et al.*[1] They pointed out that there are both fundamental and technical effects associated with alignment variations. Fundamentally, misalignments will give rise to a pulling of the resonance frequency of the resonator, an issue we discuss further below. Sanders *et al.* also observed pulling effects associated with spatial nonuniformities of the sensitivity of the detector used to monitor the output of the resonator and from which an error signal was derived. Hough *et al.*[2] have measured the frequency shifts associated with angular changes of a beam injected into a reference cavity and have estimated their effect on the frequency stability of a dye laser.

Difficulties associated with laser beam alignment have led a number of groups to study the possible means of alignment stabilization. Rudiger *et al.*[3] on a passive approach to the problem found that a passive resonator, placed between the source laser and a resonant interferometer, transmits the fundamental spatial mode of the resonator while suppressing the transverse modes. Their system demonstrated considerable reduction of alignment fluctuations that originated from the source laser. This passive mode suppressor, however, does not eliminate changes in alignment that originate after the mode suppressor. An active laser beam position stabilization technique is described by Grafstrom *et al.*[4] Their method employs two quadrant photodiodes that monitor the position of a laser beam at two locations, thereby providing both tilt and transverse displacement information. Although it is simple to implement, the technique does not directly monitor the relationship between the cavity optical axis and the input beam. The demonstration given here is based on an earlier proposal by one of us (D.Z.A.) for active control of beam alignment.[5] This technique directly monitors the presence of cavity off-axis modes, which are indicative of misalignments, by a heterodyne method that monitors the light transmitted by the reference cavity. The gravitational wave interferometer at the California Institute of Technol-

The authors are with Joint Institute for Laboratory Astrophysics, University of Colorado, Boulder, Colorado 80309-0440.

Received 16 August 1988.
0003-6935/90/030394-10$02.00/0.

ogy also employs a heterodyning scheme that monitors the light reflected from the resonator.[6] Sayeh *et al.*[7] present a treatment on the theory of mode coupling similar to ours,[5] then outline a method of alignment that frequency scans the input beam and monitors the off-axis mode coupling by direct detection.

The principles of our system are reviewed in Sec. II, where we also present an analysis of the error signals that are subsequently used to servo control the alignment. The control system is described in Sec. III. In Sec. IV we give the results of performance measurements of the implemented system. We conclude in Sec. V by relating our alignment system performance to source laser frequency stability.

II. Operating Principles

We describe the principles of operation of this alignment scheme briefly here; see Ref. 5 for greater detail. We also give an analysis of the transmitted optical signal and the subsequent extraction of error signals. The theoretical performance limitation of the system is given in terms of the optical power detected. We also consider the application of this technique to control mode matching.

A. Theoretical Review

An optical resonator has a complete set of spatial transverse electromagnetic modes (TEM), which can be represented in the paraxial beam approximation by the Hermite-Gaussian functions of the transverse coordinates x and y.[8] These eigenmodes are specified by three integral mode numbers (q,m,n). The axial mode number q (a large integer) identifies the longitudinal modes and indicates the number of waves in a round trip path of the cavity; m and n are the transverse mode numbers for the x- and y-axes, respectively.

The Hermite-Gaussian functions form a complete set of orthonormal basis functions and are a good approximation to the eigenmodes of a practical resonator even though the resonator has a finite transverse extent.[8] An arbitrary paraxial transverse field distribution can be represented as a linear superposition of these modes[9–11]:

$$\Psi(x,y) = \sum_{m=0}^{\infty}\sum_{n=0}^{\infty} C_{mn}U_{mn}(x,y), \tag{1}$$

where $\Psi(x,y)$ is the normalized input field, the U_{mn} are the basis functions of the resonator, and the C_{mn} are the coupling coefficients to the respective off-axis modes. For simplicity we consider the field distributions near the beam waists so that they are nearly plane waves and we need not consider their longitudinal (z) dependence. For each family of transverse modes there exists a longitudinal or fundamental mode, specified as $(q,0,0)$, which has a purely Gaussian profile. The profile of the transverse modes is a Gaussian that is spatially modulated by the Hermite polynomials of the transverse coordinates. The transverse spatial distribution for the Hermite-Gaussian functions evaluated at the beam waist and normalized over the infinite transverse plane has the form

$$U_{mn}(x,y) = \left(\frac{2}{\pi 2^m 2^n m!n!}\right)^{1/2} H_m\left(\frac{\sqrt{2}x}{w_{0x}}\right) \times H_n\left(\frac{\sqrt{2}y}{w_{0y}}\right)\exp\left(-\frac{x^2}{w_{0x}} - \frac{y^2}{w_{0y}}\right). \tag{2}$$

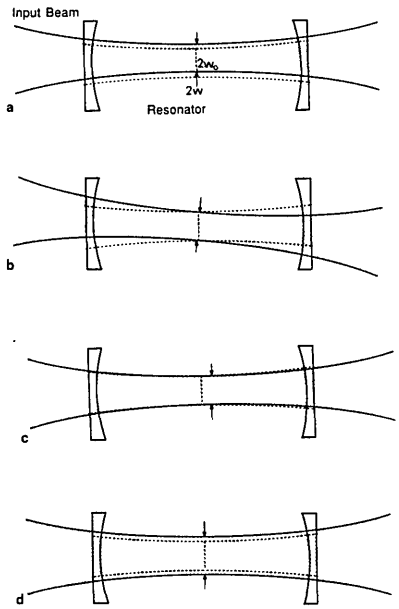

Fig. 1. Profile of laser beam injected into an optical resonator for each of the four possible alignment error types. The waist of the input beam is indicated by the arrows and the waist of the cavity by the vertical dotted line. Error types can by classified by the relative sizes and positions of the waists alone: (a) transverse beam displacement; (b) angular displacement of input beam; (c) longitudinal waist displacement; (d) waist size mismatch.

We consider a system in which the source laser operates in a longitudinal mode producing a Gaussian beam that is nominally aligned and mode matched to an optical resonator. In these conditions, the bulk of the power of the input beam is coupled to a fundamental mode, which is maintained on resonance by a servo system, and only a small fraction of the input beam power is coupled to the off-axis modes, predominately to the two lowest-order modes.

It is useful to put the beam cavity coupling errors into two classes: alignment errors and mode matching errors. These are most simply described in terms of the relative positions, orientations, and sizes of the waists of the input beam with respect to those of the cavity. The waist of a Gaussian beam is where the cross section is smallest and the wavefront is planar. The size and shape of the waist (or waists) of an optical resonator are determined by its geometry. The various misalignments are depicted in Fig. 1. When perfectly aligned and mode matched the two waists coincide exactly, and all input light couples solely to the fundamental mode.

Small misalignments and mode mismatches have the property that each type couples primarily to the two lowest orders of off-axis modes, as in the approximation

$$\Psi(x,y) \approx C_{00}U_{00}(x,y) + C_{10}U_{10}(x,y) + C_{01}U_{01}(x,y) + C_{20}U_{20}(x,y) + C_{02}U_{02}(x,y), \quad (3)$$

where $U_{00}(x,y)$ is the fundamental mode, $U_{10}(x,y)$ [$U_{01}(x,y)$] is the first-order off-axis mode in the x-direction (y-direction), and $U_{20}(x,y)$ [$U_{02}(x,y)$] is the second-order off-axis mode in the x-direction (y-direction). We can neglect the mixed terms such as $U_{11}(x,y)$ since they are of second or higher order in the misalignments.

Alignment errors correspond either to lateral displacements of the input beam waist [Fig. 1(a)] relative to that of the cavity or to angular tilts between the planes of the two waists [Fig. 1(b)]. Both alignment error types cause coupling primarily to the first-order transverse modes. For an arbitrary misalignment both the U_{10} and U_{01} modes are excited, the admixture of modes being determined by the orientation of the misalignment. A linear cavity with nonastigmatic mirrors ideally has no preferred transverse axis. However, for a planar ring cavity with spherical mirrors, it is convenient to define the transverse axes such that one is in the plane of the resonator and the other is normal to it.

Mode mismatches correspond to longitudinal displacements [Fig. 1(c)] or size differences [Fig. 1(d)] between the waists and give rise to coupling chiefly to second-order off-axis modes. For the case of the nonastigmatic resonator with a radially symmetric input beam, a mode mismatch would couple equally to both the U_{02} and U_{20} modes generating a bull's-eye shaped mode distribution.[7]

Each eigenmode has an associated resonant frequency; these frequencies are in general nondegenerate. For a resonator with two spherically curved mirrors, the separation frequencies between off-axis modes and the fundamental mode are given by[8]

$$\Delta\nu_{mn} \approx \frac{\nu_s}{\pi}\left\{m \arccos\left[\left(1-\frac{L}{2f_{1x}}\right)\left(1-\frac{L}{2f_{2x}}\right)\right]^{1/2} + n \arccos\left[\left(1-\frac{L}{2f_{1y}}\right)\left(1-\frac{L}{2f_{2y}}\right)\right]^{1/2}\right\}, \quad (4)$$

where ν_s is the longitudinal mode separation frequency ($\nu_s + c/n_0L$; L is the length of the round-trip optical path of the resonator, and n_0 is the refractive index of the intracavity medium). The sign of the square root is that of $1 - L/2f_{1\mu}$ ($\mu = x,y$), which is equal to that of $1 - L/2f_{2\mu}$. The remaining parameters are defined as follows: f_{1x} and f_{2x} (f_{1y} and f_{2y}) are the focal lengths of the mirrors in the x-axis (y-axis), and m and n are the orders of the modes in the x and y directions. The resonant frequencies of a more general resonator are calculated by Collins.[12]

In what follows we consider a control system that corrects only for the alignment class of errors. Table I lists the amplitude coupling coefficients to first-order off-axis modes for the four possible input beam alignment errors.

The beam waists $w_{0\mu}$ can be evaluated using

$$w_{0\mu}^4 = \left(\frac{\lambda}{\pi}\right)^2 \frac{(2f_{1\mu} - L)\,(2f_{2\mu} - L)\,[2(f_{1\mu} + f_{2\mu}) - L]}{4(f_{1\mu} + f_{2\mu} - L)^2}. \quad (5)$$

Here $\alpha_{0\mu}$ are the far-field divergence angles of the beam and are given by

$$\alpha_{0\mu} = \frac{\lambda}{\pi w_{0\mu}}. \quad (6)$$

Measurements of all four of the coupling coefficients determine the orientation of the beam with respect to the cavity waist.

B. Derivation of Error Signals

The alignment error signals are obtained by an optical heterodyne technique. Phase modulation sidebands are applied to the laser beam at the frequencies separating the first-order off-axis mode from the fundamental. The horizontal and vertical off-axis modes of the nonastigmatic linear resonator are degenerate and so have the same frequencies. In such a case only one phase modulation frequency need be applied. However, an astigmatic resonator, such as a ring resonator with spherical mirrors, requires a separate set of sidebands for each of the two first-order mode frequencies. In the following description and analysis of the optical and electrical error signals, we consider only misalignments in the x-direction; the analysis for the y-dimension is entirely the same:

The field amplitude for a beam of phase modulated light at the optical frequency ω has the form

$$\mathbf{E}_{pm} = \mathbf{E}_o\left\{\sum_{k=0}^{\infty} J_k(m)\,\exp[i(\omega + k\omega_m)t] + \sum_{k=1}^{\infty}(-1)^k J_k(m)\,\exp[i(\omega - k\omega_m)t]\right\}, \quad (7)$$

where ω_m is the modulation frequency, $\mathbf{E}_o$ is a constant real vector, and $J_k(m)$ is the Bessel function of order k and phase modulation index m. In this notation, the physical electric field is obtained by taking the real part of the complex quantities. Figure 2(a) shows the spectrum of the electric field of the phase modulated input beam.

The transmission spectrum of a misaligned resonator is shown in Fig 2(b). Since the carrier is locked to the fundamental mode frequency, much of the optical

Table I. Coupling of Off-Axis Modes Due to Cavity Misalignments

Degree of freedom	Misalignment parameter	Coupling coefficient	Phase (deg)	Frequency	Mode
x-translation	a_x	a_x/w_{0x}	0	ν_{10}	U_{10}
x-tilt	α_x	α_x/α_{0x}	90	ν_{10}	U_{10}
y-translation	a_y	a_y/w_{0y}	0	ν_{01}	U_{01}
y-tilt	α_y	α_y/α_{0y}	90	ν_{01}	U_{01}

power in the carrier is transmitted by the cavity. In this case, the first upper sideband is also at a cavity resonance, that of the first-order off-axis mode. Only the light that is coupled by misalignment into the first-order off-axis mode at the upper sideband frequency can resonate. Such light is transmitted with the field distribution of the off-axis mode by an amount proportional to the extent of the misalignment. This is represented by the spectrum shown in Fig. 2(c). The optical components at the frequencies of the lower sidebands are nonresonant, and so they are primarily reflected by a high finesse cavity.

The field amplitude of the transmitted beam is approximated by

$$\mathbf{E}_t \approx \mathbf{E}_0 t_c \{C_{00} J_0(m) \exp(i\omega t U_0)(x) + C_{10} J_1(m) \exp[i(\omega + \omega_m) t U_1](x)\} U_0(y), \quad (8)$$

where we have neglected nonresonant fields and weak coupling to higher-order modes. Here t_c is the transmitivity of the cavity on the fundamental mode resonance. The transmitted beam consists mainly of the fundamental mode (coupling coefficient $C_{00} \approx 1$) at the carrier frequency but with a small contribution from the first-order off-axis mode ($C_{10} \ll 1$) at one of the sideband frequencies. The resulting transmitted intensity exhibits spatially dependent amplitude modulation at the beat frequency ω_m as follows:

$$\begin{aligned} I_t(x,y) &= \mathbf{E}_t^* \cdot \mathbf{E}_t \\ &= T_c E_0^2 \left\{ |C_{00}|^2 J_0^2(m) U_0^2(x) + |C_{01}|^2 J_1^2(m) U_1^2(x) \right. \\ &\quad + 2 J_0(m) J_1(m) U_0(x) U_1(x) \\ &\quad \left. \times \left[\frac{a}{x_0} \cos\omega_m t - \frac{\alpha}{\alpha_{x0}} \sin\omega_m t \right] \right\} U_0^2(y). \end{aligned} \quad (9)$$

The transmission of the cavity is $T_c = |t_c|^2$. For a nearly aligned system, the first term is a large constant term; the second term is constant but small and can be neglected since it is second order in the misalignment. The third term is the one of interest, for it represents amplitude modulation of the transmitted beam at the modulation frequency and is proportional to the transverse mode coupling amplitude.

Detection of the transmitted beam at the modulation frequency provides the alignment information. The translational and angular errors are retrievable independently, as each is proportional to one of two quadratures of the rf signal. Since the Hermite-Gaussian functions are mutually orthogonal when integrated over all space, detection of the entire transmitted beam by a single element results in only a dc signal. The field distribution of the first-order off-axis mode is antisymmetric about its transverse axis, whereas the fundamental mode is symmetric. Consequently, the strongest signal is obtained by separate detection of each half of the transmitted beam, followed by electronic subtraction of the two photocurrents. The photocurrent of a signal detected by a two-element, differential detector (where the whole

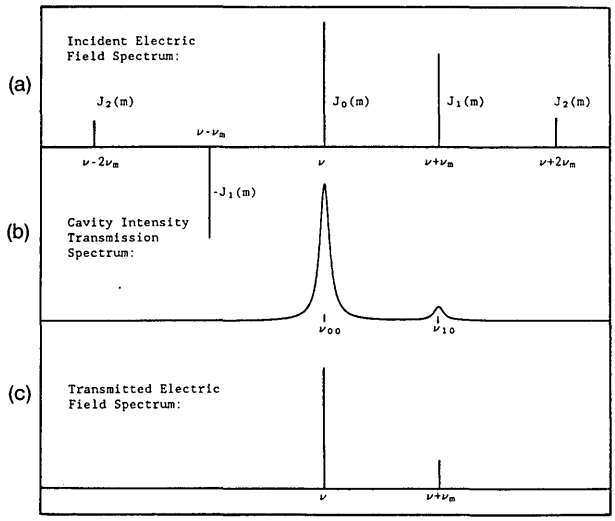

Fig. 2. Frequency spectra of electric fields and cavity transmission. In normal conditions the input beam carrier frequency is locked to the cavity fundamental mode frequency $\nu = \nu_{00}$. The beat of the two transmitted frequencies produces the rf alignment error signals: (a) electric field of phase modulated input beam; (b) transmission of resonator; (c) electric field of transmitted beam.

detector is significantly larger than the beam's spot size) is approximately

$$\begin{aligned} i_{\text{det}} &\approx \frac{e\eta}{h\nu} \int_{-\infty}^{\infty} dy \left\{ \int_{o}^{\infty} I(x,y)dx - \int_{-\infty}^{o} I(x,y)dx \right\} \\ &\approx \left(\frac{2}{\pi}\right)^{1/2} \left(\frac{2e\eta\lambda}{hc}\right) P_0 T_c J_0(m) J_1(m) \\ &\quad \times \left[\frac{a}{x_0} \cos\omega_m t - \frac{\alpha}{\alpha_{x0}} \sin\omega_m t \right], \end{aligned} \quad (10)$$

where P_0 is the laser power incident on the resonator, η is the quantum efficiency of the detector, and λ is the optical wavelength. The charge of the electron is represented by e, the speed of light by c, and Planck's constant by h. Equation (10) shows that the intensity modulation that is in-phase with the modulation is proportional to the translational error and the quadrature signal is proportional to the angular alignment error.

The use of a quadrant photodetector permits efficient simultaneous detection of coupling to both vertical and horizontal off-axis modes. With this detection geometry the signals from the four elements must be summed and differenced electronically. A more detailed description of the quadrant detector is given in Sec. VI. The alignment system could alternatively be incorporated with a single element detector in place of any one of the quadrant elements and still obtain all the necessary information. The drawback in that case is a 12-dB reduction in signal (6-dB reduction in signal-to-noise for shot noise limited detection) compared to the quadrant detector geometry.

This heterodyne alignment scheme has the attractive feature that the zero of the error signal is independent of the location of the transmitted spot with re-

spect to the photodetector for small deviations from center. If the transmitted beam is not centrally located on the quadrant photodetector, a reduction of error signal strength occurs, not a systematic offset. The beam position is monitored in the test system by measuring the imbalance of the photocurrents of the quadrant detector. When the photocurrents are equal the detector is properly located, assuming that the detector is moderately homogeneous and imbalances in the dark currents are small. Only occasional adjustment of the detector position is necessary.

Isolation of the translational errors and angular errors from a common rf signal is possible because the two errors are manifest in conjugate quadratures of the heterodyned signal. The rf phase of the amplitude modulation of the transmitted beam is in-phase with the applied modulating field for transverse displacements and waist size mismatches, and in-quadrature (90° out of phase) for angular tilts and longitudinal waist translations. Thus selecting the proper demodulation phases allows one to obtain all error signals simultaneously and independently. These error signals are fed back to transducers that appropriately correct the beam position and angle.

C. Noise Limitation

Detection sensitivity to the misalignments is theoretically limited by the shot noise of the photocurrent. The total dc photocurrent can be found by integrating the first term of Eq. (8) yielding

$$i_{dc} \approx \eta \frac{e\lambda}{hc} T_c P_0 J_0^2(m), \tag{11}$$

which gives the rms shot noise current

$$i_{sn} \approx \left[2 \frac{\eta e^2 \lambda}{hc} T_c P_0 J_0^2(m) \Delta f \right]^{1/2}, \tag{12}$$

where Δf is the bandwidth of the measurement. Thus we find that the best achievable SNR is

$$\left(\frac{S}{N}\right)_{\max} = \frac{\langle i_{\omega_m} \rangle^2}{i_{sn}^2} \approx \frac{\eta\lambda}{\pi hc} \frac{P_0 T_c J_1(m)}{\Delta f} \left[\frac{\langle a^2 \rangle}{x_0^2} + \frac{\langle \alpha^2 \rangle}{\alpha_{x0}^2} \right]. \tag{13}$$

where $\langle a^2 \rangle$ and $\langle \alpha^2 \rangle$ are the variances of translational and angular fluctuations and it is assumed that $a(t)$ and $\alpha(t)$ vary slowly compared with $1/\omega_m$ and we define their average values to be zero. This performance limit can be expressed as the ratio of minimum power coupled to the transverse mode P_{10} to the power in the fundamental mode P_{00}:

$$\left(\frac{P_{10}}{P_{00}}\right)_{\min} \approx \frac{\langle a^2 \rangle}{x_0^2} + \frac{\langle \alpha^2 \rangle}{\alpha_{x0}^2} \approx \frac{\pi hc \Delta f}{\eta \lambda P_0 T_c J_1^2(m)}. \tag{14}$$

In the limit of small modulation index Eq. (13) takes the form

$$\left(\frac{P_{10}}{P_{00}}\right)_{\min} \xrightarrow[m \ll 1]{} \frac{4\pi hc \Delta f}{\eta \lambda P_0 T_c m^2}. \tag{15}$$

Although $J_0(m)$ does not appear in Eqs. (14) and (15), we have assumed that the optical power in the carrier coupled to the longitudinal mode is greater than that of the off-axis modes.

D. Extension to Mode Matching

This paper describes a system for the automated control of alignment. However, mode matching can also be actively controlled if necessary. In this section we briefly discuss how the system could be so expanded.

Incorporation of active mode matching is a straightforward extension of this alignment system. It would be appropriate in cases in which the dominant cause of frequency drift is due to fluctuations in the coupling to second-order off-axis modes. Such an extension of the system involves either phase modulating at a frequency near the second harmonic of the first-order separation frequencies or, more practically, modulating at the first-order off-axis mode frequency with sufficient excursion to produce substantial second-order sidebands. The detector geometry needs to be modified to separate the inner and outer annular regions of the beam at the zero crossing of the second-order mode field distribution, perhaps by the use of a bull's-eye shaped eight-element photodetector, four quadrants inside an annular ring of four more quadrants.

III. Apparatus

Figure 3 shows the apparatus used to demonstrate the principle of the alignment scheme and to measure its performance. We describe the source laser and its frequency control system in Sec. III.A. Two types of detector were used for the 1-D and 2-D alignment systems with two and four degrees of freedom, respectively. The 1-D detector demonstrates slightly better performance and is described in Sec. III.B. A quadrant detector used to demonstrate simultaneous vertical and horizontal beam control is described in Sec. III.C. The feedback system including beam-steering mirrors and their controllers is described in the final subsection.

A. Laser and Frequency Control System

A polarized, single frequency He–Ne laser at 633 nm produces a source beam with an output power of 400 μW. The laser frequency is locked to the fundamental mode of the passive Zerodur cavity by means of a phase modulation technique using the reflected optical signal.[13] A piezo-backed resonator mirror controls the frequency of the reference cavity and has a dynamic range of more than one free spectral range. Long-term frequency stabilization is achieved by controlling the current through a small heater foil on a small end portion of the laser tube, thus controlling the laser cavity length and frequency. Fast servo response is achieved by controlling the laser discharge current.[14]

The ring resonator is a square cavity, 7 cm on a side, with a longitudinal mode finesse of ~360 and an intensity transmission of ~65% on resonance. The input mirror and its diagonally opposed output mirror are flat. The other two mirrors are spherically concave. Two $LiTaO_3$ crystals of dimensions ($h \times w \times l$) of $3 \times 3 \times 25$ mm are used to apply phase modulation sidebands at ~60 and 83 MHz, which correspond to the

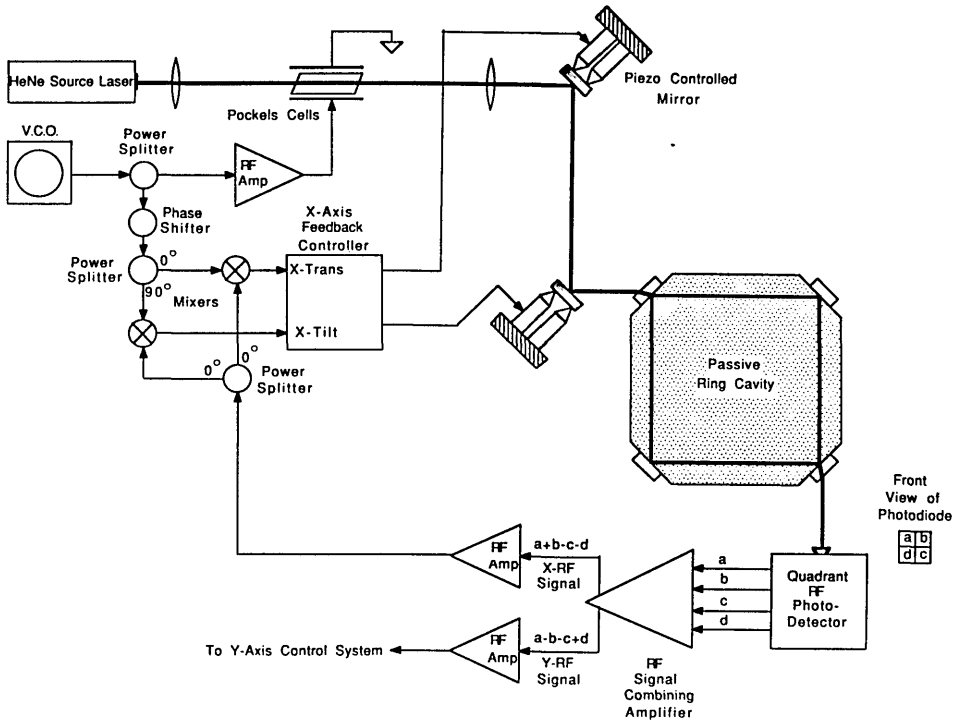

Fig. 3. Block diagram of 1-D two degrees-of-freedom alignment system.

separation frequencies of the off-axis modes of the passive ring cavity. The lower frequency is that of the out-of-plane axis referred to here as the x-axis, and the higher frequency is that of the in-plane axis or y-axis. The lower modulation frequency is used not only for alignment but also for laser frequency stabilization. The phase modulation indices are both ~0.7.

B. One-Dimensional Detector

The beam transmitted by the resonator contains all the alignment error information. A two-element high speed detector is used to test the performance of a 1-D, two-degrees-of-freedom alignment system that corrects tilt and translational errors in the x-axis (vertical axis) only. The detector utilizes two adjacent channels of a quadrant photodiode. The photocurrents are amplified by two low noise dual gate FET-input preamplifiers. These signals are then subtracted by an rf power combiner.

C. Two-Dimensional Detector

For optimal performance in a four degrees-of-freedom alignment system that controls beam alignment in both vertical and horizontal axes, a quadrant photodetector is used. Each element has its own low noise preamplifier; two of each are housed in separate chambers of a segmented, shield housing. Another chamber houses the signal combining amplifier. A fourth chamber contains the dc signal combining circuitry. Channel separation of 35 dB was measured by applying an amplitude modulated optical signal to one quadrant and measuring the signal strength in the others.

If we label the four detector elements a, b, c, and d in a clockwise manner, the rf error signals required by the servo are $a+b-c-d$ and $a-b-c+d$. The four preamplifier outputs are amplified, summed, and differenced by a combination of low noise rf amplifiers used with rf transformers to provide the appropriate signs. Figure 4 shows a basic schematic of the 2-D detector. The relative gains and phases of the four quadrant amplifiers are adjusted to give the best cancellation of signals. The outputs are two independent rf signals, the amplitudes of which are proportional to the couplings to the two first-order transverse modes. The rf signals are amplified an additional 13 dB before being phase shifted and demodulated. In the test system demodulation is accomplished by the use of two mixers and 0 and 90° power splitters as shown in Fig. 3 to provide the four requisite error signals.

D. Feedback Controllers and Beam Steering Mirrors

Feedback to the beam orientation is accomplished by tilting the mirrors (shown in Fig. 3), both horizontally and vertically, with piezoelectric transducers. Each mirror controller consists of two cone-capped piezotubes (l = 25.4 mm, o.d. = 6.35 mm, t = 0.51 mm) and one identically shaped solid ceramic cylinder. The back side of the mirror is held against the apexes of the three caps by a spring fastened at one end to the mirror and at the other end to the base of the mirror mount. The voltage required to move the beam through its far-field divergence angle, which is considerably more than even the largest of observed fluctuations, is ~220 V. Lateral translations of the beam are generated by tilting two mirrors separated by 30 cm

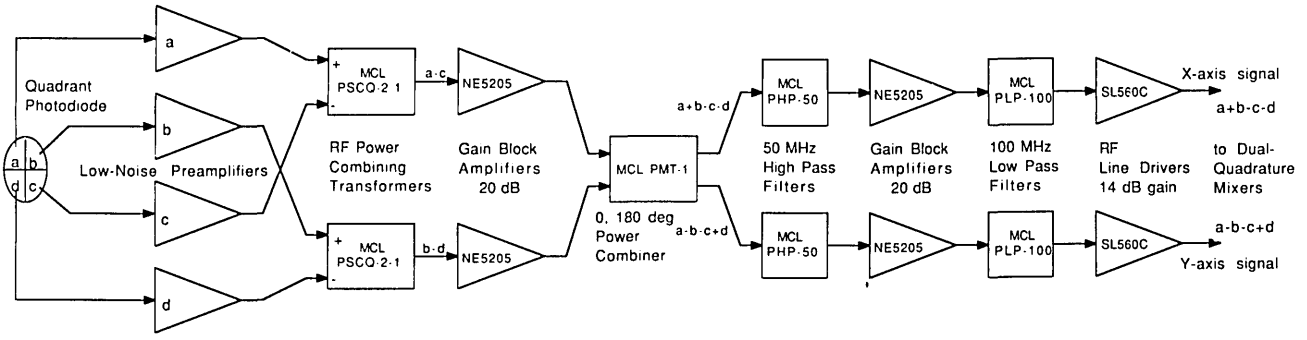

Fig. 4. Block diagram of 2-D detector used to derive the rf error signals for the four-degrees-of-freedom alignment system.

through nearly identical angles. With this configuration a piezovoltage of ~780 V would be needed to translate the beam through a distance equal to one beam waist.

The symmetry of the ring resonator fixes the cavity waist positions at the input and output mirrors of the cavity. Nearly pure tilts of the waist of the injected beam (with respect to the cavity waist) are produced by a piezomounted mirror $M1$ positioned close to the input mirror, whereas translations are generated using the combined motion of both mirror $M1$ and another mirror $M2$ located some distance back toward the source laser along the beam path (Fig. 3).

The two means of feedback need not be pure tilt and pure translation provided that the two actions are nearly orthogonal combinations of the two. These relative amplitudes are given below as a function of the phase of the local oscillator ϕ:

$$\text{in-phase:} \quad \frac{a}{x_0}\cos\phi - \frac{\alpha}{\alpha_{0x}}\sin\phi,$$

$$\text{in-quadrature:} \quad \frac{a}{x_0}\sin\phi + \frac{\alpha}{\alpha_{0x}}\cos\phi.$$

The error signals generated by the in-phase and in-quadrature demodulation of the rf signals are filtered and amplified before being fed to the high voltage piezoamplifiers that control the mirrors. The groups of amplifiers used for this task are referred to in Fig. 3 as feedback controllers. They are broken down into their functional components in Fig. 5.

The beam waist of the test cavity is positioned at the flat input mirror. The tilt mirror stands ~2 cm before the input mirror. Although its motion primarily produces tilts, slight translation of the beam occurs as well. A procedure for orthogonalizing these motions is described as follows:

An error signal, or test signal, is produced by applying a large sinusoidally varying voltage to the tilt piezo. The error signals induced and demodulated in both quadratures can be effectively displayed on an oscilloscope in the X-Y mode while the system operates open loop. Simultaneous adjustment of the phases of both local oscillator signals is accomplished by means of a common phase shifter (while keeping the relative phase difference constant at 90°) shown in Fig. 3, thus

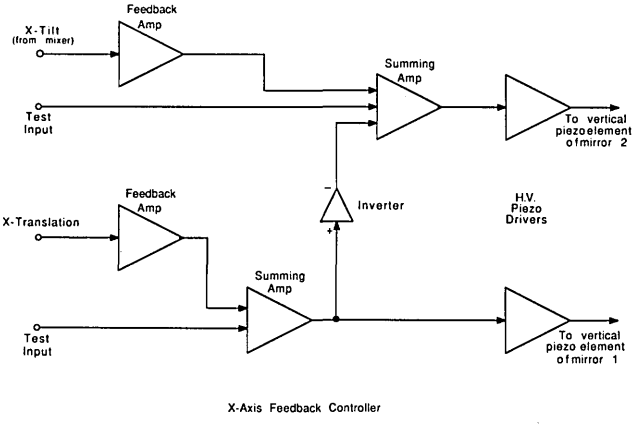

Fig. 5. Block diagram of mirror control amplifiers.

allowing one of the induced error signals to be maximized while simultaneously nulling the other. The maximized signal corresponds to a tilt motion perhaps with some slight translation. The nulled signal corresponds to the orthogonal combination of motions, primarily translation. The motion corresponding to the nulled signal can be constructed by tilting both mirrors in combination and adjusting the relative gains of the high voltage amplifiers so that the previously nulled signal (translational signal) is maximized, and the tilt signal is nulled. The same process is used in both dimensions, thus generating the four mutually orthogonal signals that correspond to the four combined motions of the alignment mirrors. Amplification and feedback of these error signals provide for the correction of all possible alignment errors.

IV. System Performance Measurements

The performance of the alignment servo system can be determined by making three measurements: (1) measurement of the quadrant detector noise; (2) calibration measurements of error signals; and (3) open and closed loop error signal noise measurements. We present here the results for a two-degrees-of-freedom alignment system that corrects x-tilt and x-translation errors only. We have obtained comparable results for four and eight-degrees-of-freedom alignment systems, the latter system controls alignment of both clockwise

and counterclockwise beams injected into a ring resonator. In these systems the signal to noise is somewhat reduced by the reduction of optical power in the carrier by the imposition of two sets of phase modulation sidebands and to the splitting of the source beam into two directions in the eight-degrees-of-freedom system.

A. Detection Noise

Each element of the two-channel detector has a noise equivalent current of 35 μA at 60 MHz. This photocurrent corresponds to the shot noise of 80 μW of optical power per channel at 633 nm. The noise was measured by applying a white light source to increase the noise level from the preamplifiers by 3 dB over the amplifier noise level, as measured in the noise spectral density of the error signal. The total power of the light transmitted by the test cavity is 160 μW, which is the same as the noise equivalent power of the detector. Therefore, the noise of the detection system is equal to the shot noise of the transmitted beam, and the error signal detection is nearly shot noise-limited.

B. Calibration

Calibration of tilt error signals is accomplished by tilting the mirrors through measured displacements and determining the associated error signal change while operating open loop. Translations were generated by passing the input beam through a 6.35-mm quartz parallel and tilting the parallel through small measured angles.

C. Error Signal Noise

Noise measurements of the error signals are made on an audio frequency spectrum analyzer. The noise power spectral density of the error signal gives a measure of the fluctuations in beam angle and the effectiveness of the servos in correcting for these fluctuations. The open and closed loop noise measurements are shown in Figs. 6 and 7 for translational and angular fluctuations, respectively. In the open loop measurement the low frequency noise is seen to increase dramatically above the instrument noise and shot noise below 30 Hz. The noise spectral density due to the instrument and shot noise is represented by the flat horizontal curve. This level corresponds to 0.08 nm/$\sqrt{\text{Hz}}$ for the translational errors and 0.1 nrad/$\sqrt{\text{Hz}}$ for tilt errors and represents the performance limit of this alignment system.

In terms of the coupling coefficients these values correspond to 2 parts in $10^7/\sqrt{\text{Hz}}$ each, yielding an off-axis mode power of -131.0 dB for a 1-Hz bandwidth. The noise at ~12 Hz is due to acoustical noise from the building ventilation system. Sharp spikes are observed at the 60-Hz line frequency and its harmonics. These could be reduced by improving power supply filtering or operating on batteries.

The lowermost traces in Figs. 6 and 7 are the closed loop noise measurements of the error signal. These

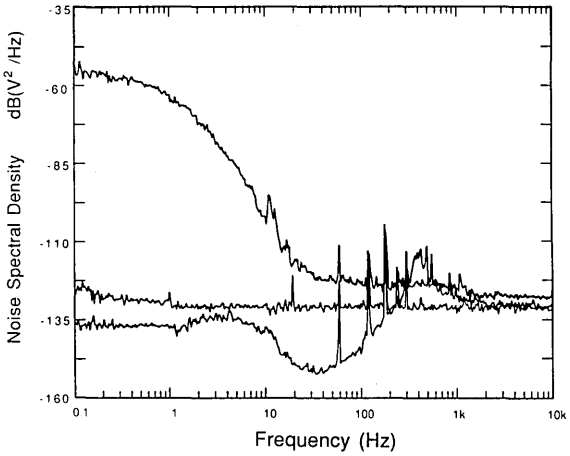

Fig. 6. X-axis translational error signal noise measurements from 0.1 Hz to 10 kHz. The uppermost trace indicates the extent of the open loop alignment fluctuations. The next lower trace indicates the noise level caused by both the instrument noise and shot noise that results when white light producing the same photocurrent as the transmitted beam is incident on the detector. This represents the actual performance limit. The closed loop response is given by the lowest curve.

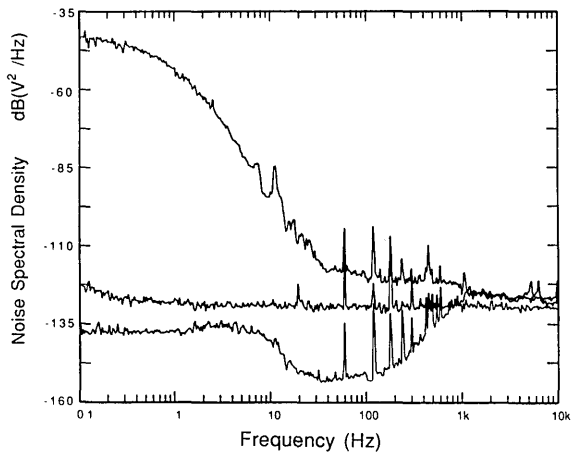

Fig. 7. X-axis angular error signal noise measurements from 0.1 Hz to 10 kHz.

spectra show noise reduction by 80 and 90 dB at low frequencies, reducing the power spectral density below the instrument noise level of the detector assembly. This does not indicate alignment performance beyond the instrument noise level, but rather, that the servos impose the instrument and shot noise onto the alignment to maintain a null at the mixer output. The noise corner of the low frequency noise is less than 1 Hz and is dominated by the $1/f$ noise of the mixer. Above this frequency white instrument noise is the dominant source.

For comparison, we can calculate the shot noise limit of alignment system performance using Eq. (13). For our test system, the cavity transmission T_c is 60%, the incident power P_0 of red light (633 nm) is 400 μW, the quantum detection efficiency η is nominally 80%, and the modulation index m is 0.75 providing a total photo-

current of 70 μA. The coupling to the off-axis mode for a 1-Hz bandwidth measurement, if shot noise limited, would be −132 dB, relative to the fundamental mode. The measured alignment fluctuations are within 2 dB of that shot noise limit. This is approximately what we expect considering that the detection noise is approximately equal to the optical shot noise.

D. Error Sources

In the alignment system the two primary sources of systematic errors are dc offsets in the error signals and rf pickup in the detected signals before the mixers. The dominant sources of dc offsets are the output offset voltages of the mixers, rated at 200 μV, and the input offset voltages of the feedback amplifiers, rated at only 10 μV. Compensation of the biases is achieved by the addition of an equal but opposite dc signal after the first stage of amplification. These offsets are nulled by either of two methods. One method is to null the detected rf components while monitoring the rf signal on an rf spectrum analyzer as the alignment system runs closed loop. The other simpler technique is to display the error signals in the x-y mode on an oscilloscope and to compare the closed loop position of the scope trace with its position when the light to the detector is blocked. When the two positions coincide the offsets are nulled. Proper adjustment of the offsets reduces the rf signals detected at modulation frequencies to below the background noise levels in surrounding frequency regions.

The rf pickup affects the servo in an analogous way to dc offsets, as the servo can null an arbitrary rf signal by adding an equal and opposite one, while inducing an alignment error. Pickup can be detected by monitoring the rf signal while blocking the beam to the detector.

One difficulty of this system is that periodic adjustments are required to compensate for drifts associated with the dc offsets of the mixers and the relative rf phases. Drifts in phase shifts in the test system are primarily a result of drifts in the frequencies of the local oscillators or in the geometry of the reference cavity. The latter changes the separation frequencies of the off-axis modes. For this reason the temperature of the reference cavity has been stabilized. Another source of off-axis mode frequency drift is the piezo-backed mirrors used for frequency control. Changes in the mirror displacement alter its effective curvature, which in turn causes the off-axis mode resonance frequencies to change. This effect has been measured as high as 0.5 MHz per free spectral range. The extent of these drifts can be minimized by the use of stable oscillators, high rf gain, high quality mixers (i.e., with low $1/f$ noise), and temperature-controlled circuitry and cavity geometry.

V. Conclusions

We have found that this alignment system can suppress alignment noise and reduce coupling amplitudes to the first-order transverse modes by as much as 80 dB. The spectral density of the translational and angular fluctuations in the test system were measured to be about 2 parts in $10^7/\sqrt{\text{Hz}}$ in both the beam waist size and far-field divergence angle, respectively. This level corresponds to coupling power of several parts in 10^{14} for a 1-Hz bandwidth measurements.

The extent of frequency pulling can be estimated by calculating the detuning for which the transmitted intensity is maximized. We can calculate the detuning as a function of off-axis mode coupling amplitude by adding the transmitted fields and finding the maximum in total integrated power. In principle, the cross-term should vanish due to the orthogonality of the modes; however, in practice nonhomogeneous detection provides a significant contribution from the cross term. As demonstrated by Meyer *et al.*[15] the cross-term component usually dominates the pulling. By a method similar to that of Meyer, we estimate the frequency pulling due to coupling to the U_{10} mode at 60 MHz is a few tens of microhertz for a 1-Hz measurement for the test cavity when the alignment is stabilized, assuming a 1% asymmetry in the mode cancellation.

Comparing the stabilization limit using the phase modulation technique of Drever *et al.*[13] we find that for a 400-μW reflected beam at a phase modulation frequency six times the linewidth, the shot-noise-limited frequency fluctuations would be ~800 μHz for a 1-Hz measurement bandwidth. We conclude that with such an alignment scheme controlling alignment in both axes, the alignment dependent frequency fluctuations are suppressed below the limits of laser stabilization technique. Without the alignment system in operation the alignment fluctuations of the test system are ~10,000 times greater (at 1 Hz) and would contribute to frequency fluctuations well above the shot noise level.

The reference cavity used in this experiment is one of modest finesse; higher finesse cavities are often employed in precision applications. To extend the arguments to cavities of higher finesse we consider the following: For a frequency discriminator in the quasistatic limit (i.e., the modulation frequency is much less than the cavity linewidth), the extent of frequency pulling for a given coupling amplitude goes as the inverse square of the resonator finesse, assuming that the pulling is dominated by the cross term. If the detector is nearly homogeneous and the term proportional to power coupled to the off-axis mode dominates the frequency pulling, the detuning will be inversely proportional to the fourth power of the finesse. The shot noise limit of the frequency discriminator goes as only the inverse of the finesse. This indicates that the frequency stability using higher finesse cavities is limited to a lesser extent by misalignments than with lower finesse resonators.

We have demonstrated the feasibility of using active control of beam alignment to suppress the coupling of an input beam to transverse modes. We expect that this system can substantially reduce frequency pulling due to first-order off-axis modes.

We gratefully acknowledge the support of Litton Corp., Guidance & Control Systems Division, and the National Science Foundation (grant PHY84-51282). Dana Z. Anderson is a Presidential Young Investigator and an Alfred P. Sloan Research Fellow.

References

1. G. A. Sanders, M. G. Prentiss, and S. Ezekiel, "Passive Ring Resonator Method for Sensitive Inertial Rotation Measurements in Geophysics and Relativity," Opt. Lett. **6**, 569–571 (1981).
2. J. Hough, D. Hils, M. D. Rayman, Ma L.-S., L. Hollberg, and J. L. Hall, "Dye Laser Stabilization Using Optical Resonators," Appl. Phys. B **33**, 179 (1984).
3. A. Rudiger, R. Schulling, L. Schnupp, W. Winkler, H. Billing, and K. Maischberger, "A Mode Selector to Suppress Laser Beam Fluctuations in Laser Beam Geometry," Opt. Acta **28**, 641 (1981).
4. S. Grafstrom, U. Harbarth, J. Kowalski, R. Neumann, and S. Noehte, "Fast Laser Beam Position Control with Sub-Microradian Precision," Opt. Commun. **65**, 121 (1988).
5. D. Z. Anderson, "Alignment of Resonant Optical Cavities," Appl. Opt. **23**, 2944–2949 (1984).
6. W. R. P. Drever and R. Spero, California Institute of Technology; private communication (1984).
7. M. R. Sayeh, H. R. Bilger, and T. Habib, "Optical Resonator with an External Source: Excitation of the Hermite-Gaussian Modes," Appl. Opt. **24**, 3756–3761 (1985).
8. H. Kogelnik and T. Li, "Laser Beams and Resonators," Appl. Opt. **5**, 1550–1567 (1960).
9. K. E. Oughstun, "On the Completeness of Stationary Transverse Modes on an Optical Cavity," Opt. Commun. **42**, 72 (1982).
10. A. E. Siegman, "Orthogonal Properties of Optical Resonator Eigenmodes," Opt. Commun. **31**, 369–000 (1979).
11. A. E. Siegman, *Lasers* (University Science Books, Mill Valley, Ca, 1986), pp. 642–652.
12. S. A. Collins, Jr. "Analysis of Optical Resonators Involving Focusing Elements," Appl. Opt. **3**, 1263–1275 (1964).
13. R. W. P. Drever, J. L. Hall, F. V. Kowalski, J. Hough, G. M. Ford, A. J. Munley, and H. Ward, "Laser Phase and Frequency Stabilization Using an Optical Resonator," Appl. Phys. B **31**, 97 (1983).
14. J. L. Hall, Ma L-S., and G. Kramer, "Principles of Optical Phase Locking: With Application to Internal Mirror He–Ne Lasers Phase Locked via Fast Control of the Discharge Current," IEEE J. Quantum Electron. (Special issue on Applications of Q.E. to Frequency Standards, Clocks, and Inertial Rotation Sensors) **QE-23**, 427 (1987).
15. R. E. Meyer, G. A. Sanders, and S. Ezekiel, "Observation of Spatial Variations in the Resonance Frequency of an Optical Resonator," J. Opt. Soc. Am. **73**, 939–942 (1983).